J. Fluid Mech. (2023), *vol*. 976, A21, doi:10.1017/jfm.2023.928

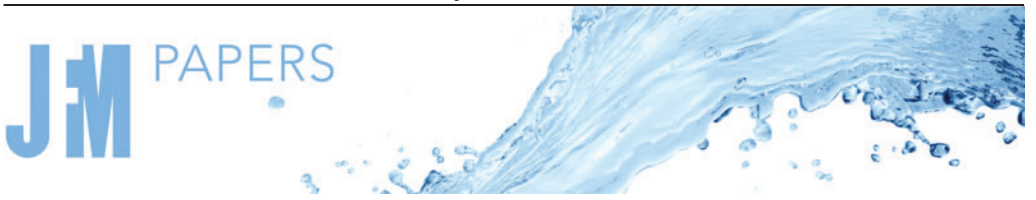

Reynolds number asymptotics of wall-turbulence fluctuations

Xi Chen[1],† **and Katepalli R. Sreenivasan**[2]

[1]Key Laboratory of Fluid Mechanics of Ministry of Education, Beihang University (Beijing University of Aeronautics and Astronautics), Beijing, 100191, PR China

[2]Tandon School of Engineering, Courant Institute of Mathematical Sciences, Department of Physics, New York University, New York, NY 10012, USA

(Received 4 June 2023; revised 23 September 2023; accepted 29 October 2023)

In continuation of our earlier work (Chen & Sreenivasan, *J. Fluid Mech.*, vol. 908, 2021, R3; Chen & Sreenivasan, *J. Fluid Mech.*, vol. 933, 2022*a*, A20 – together referred to as CS hereafter), we present a self-consistent Reynolds number asymptotics for wall-normal profiles of variances of streamwise and spanwise velocity fluctuations as well as root-mean-square pressure, across the entire flow region of channel and pipe flows and flat-plate boundary layers. It is first shown that, when normalized by peak values, the Reynolds number dependence and wall-normal variation of all three profiles can be decoupled, in excellent agreement with available data, sharing the common inner expansion of the type $\phi(y^+) = f_0(y^+) + f_1(y^+)/Re_\tau^{1/4}$, where ϕ is one of the quantities just mentioned, the functions f_0 and f_1 depend only on y^+, and Re_τ is the friction Reynolds number. Here, the superscript $+$ indicates normalization by wall variables. We show that this result is completely consistent with CS. Secondly, by matching the above inner expansion and the outer flow similarity form, a bounded variation $\phi(y^*) = \alpha_\phi - \beta_\phi y^{*1/4}$ is derived for the outer region where, for each ϕ, the constants α_ϕ and β_ϕ are independent of Re_τ and $y^* \equiv y^+/Re_\tau$ – also in excellent agreement with simulations and experimental data. One of the predictions of the analysis is that, for asymptotically high Reynolds numbers, a finite plateau $\phi \approx \alpha_\phi$ appears in the outer region. This result sheds light on the intriguing issue of the outer shoulder of the variance of the streamwise velocity fluctuation, which should be bounded by the asymptotic plateau of approximately 10.

Key words: turbulent boundary layers, turbulence theory, pipe flow

† Email address for correspondence: chenxi97@outlook.com

1. Introduction

The Reynolds number dependencies of variances of streamwise and spanwise velocity fluctuations as well as pressure are thought to present exceptional challenges for the classical notion of wall scaling (Marusic *et al.* 2010; Smits, McKeon & Marusic 2011). A salient example is that, when scaled in wall units, the peak values of these quantities near the wall grow with increasing Reynolds number over the Reynolds number range for which data are available (though the peak locations are remarkably invariant, see, e.g., Sreenivasan (1989) and § 2.1 here). In Chen & Sreenivasan (2021, 2022*a*) (together referred to as CS hereafter), the growth of these peaks was cast as a finite Reynolds number effect, and it was shown that a bounded growth model (discussed below) fits the data better. In this paper, we turn our attention to wall-normal profiles of the variances of these fluctuations. This work is an alternative to Townsend's (1956) attached-eddy hypothesis, which ascribes a logarithmic decay for fluctuations in the outer flow as

$$\phi(y^*) = B_\phi - A_\phi \ln y^*. \tag{1.1}$$

Here, ϕ represents the variance of $\langle uu\rangle^+$ or $\langle ww\rangle^+$; the superscript $+$ indicates normalization by the friction velocity $u_\tau \equiv (\tau_w/\rho)^{1/2}$ (and, where the height from the wall is involved subsequently, also by ν); u and w for fluctuation velocities in the streamwise (x) and spanwise or azimuthal (z) directions; $y^* = y/\delta$ where δ is the flow thickness; the bracket $\langle\rangle$ indicates the spatiotemporal averaging on x, z and time t ensembles; the slope A_ϕ and intercept B_ϕ are constants independent of y^* and the friction Reynolds number $Re_\tau = u_\tau\delta/\nu$, but may depend on ϕ. We do not consider $\langle vv\rangle$ here (v is the wall-normal fluctuation velocity) because it basically follows the wall-normal variation of $\langle -uv\rangle$: they both agree with the law of the wall and exhibit plateaus in the bulk region, as illustrated recently by Smits *et al.* (2021) for channel, pipe and the turbulent boundary layer (TBL), and by Yao, Chen & Hussain (2022) for the open channel.

The rationale behind (1.1), as discussed by Marusic & Monty (2019), is that the number density of the attached eddies that contribute to turbulent fluctuations varies inversely with y^*, and an integration with respect to y^* leads to the total fluctuation intensity given by (1.1). Some consequences of this idea have been explored in laboratory measurements (EXP) (Metzger & Klewicki 2001; Hultmark *et al.* 2012; Vincenti *et al.* 2013; Willert *et al.* 2017; Samie *et al.* 2018; Ono *et al.* 2022) as well as direct numerical simulations (DNS) (Wu & Moin 2009; Jimenez *et al.* 2010; Schlatter & Örlü 2010; Lee & Moser 2015; Pirozzoli *et al.* 2021; Hoyas *et al.* 2022; Yao *et al.* 2023). The resulting findings have been discussed in terms of mixed scaling (DeGraaff & Eaton 2000; Diaz-Daniel, Laizet & Vassilicos 2017), the k^{-1} velocity spectrum (Perry, Henbest & Chong 1986), a multiregime of the power-law spectrum (Vassilicos *et al.* 2015), inner–outer interactions (Marusic, Baars & Hutchins 2017) and a random addictive process (Yang & Lozano-Durán 2017). The notion of attached eddies has been extended to study high-order moments of single point velocity fluctuations (Meneveau & Marusic 2013) as well as to velocity structure functions (de Silva *et al.* 2015) and to an adverse pressure gradient boundary layer flow (Hu, Dong & Vinuesa 2023).

Pressure fluctuations have also received attention in the past (Bradshaw 1967; Klewicki, Priyadarshana & Metzger 2008; Panton, Lee & Moser 2017), in part because of their importance for aircraft cabin noise. By extending Townsend's attached-eddy hypothesis, Bradshaw (1967) obtained a k^{-1} spectrum by an inner–outer matching in wavenumber space and hence a $\ln Re_\tau$ growth of wall pressure fluctuation. The k^{-1} spectrum so deduced is marginally detected in laboratory boundary layers at $Re_\tau \approx 6000$ (Tsuji *et al.* 2007), but not in the DNS data so far. This unsatisfactory situation prompted Panton *et al.* (2017) to

develop alternative matching analysis in the spatial domain, also yielding the log profile of the type (1.1). This is reminiscent of Hultmark (2012) who derived the $\ln y$ variation in pipes by matching $\langle uu\rangle^+$ between the inner and outer regions. It is worth noting that the Re_τ effects included in these models are not part of Townsend's original attached-eddy hypothesis. To account for this, Hwang, Hutchins & Marusic (2022) revisited Townsend's model and introduced the Re_τ dependence for the proportionality coefficient A as well as the intercept B in (1.1), and revised the spectral analysis. Finally, Pullin, Inoue & Saito (2013), Laval *et al.* (2017) and Nils (2021) have suggested an additional power-law term in (1.1), which incorporates the finite Re_τ dependence.

While the work based on the attached-eddy models suggest a boundless growth of turbulence peaks as $Re_\tau \to \infty$, CS argued that the observed variations are bounded at very high Reynolds numbers and follow a defect law of the type

$$\phi_p(Re_\tau) = \phi_\infty - c_{\phi,\infty} Re_\tau^{-1/4}. \tag{1.2}$$

Here, ϕ_∞ the asymptotically bounded value of peak $\phi_p(Re_\tau)$ and $c_{\phi,\infty}$ are the fixed coefficients. We refer to CS for details but merely remark here that the underlying physics of (1.2) depends on the slight imbalance that exists between wall dissipation and maximum production in the turbulent energy budget at any finite Reynolds number, and on their tendency to eventually balance each other. Specifically, the wall dissipation falls short of the asymptotic value at finite Reynolds number by transmitting outwards an amount given by $\varepsilon_d = u_\tau^3/\eta_0$, where η_0 is the outer flow Kolmogorov length scale. This then leads to $\varepsilon_d^+ = \varepsilon_d/(u_\tau^4/\nu) \sim Re_\tau^{-1/4}$, and hence to (1.2) for wall-dissipation and other mean flow quantities. Subsequently, Monkewitz (2022) showed that an asymptotic expansion of $\langle uu\rangle^+$ profiles with the $Re_\tau^{-1/4}$ gauge function from CS reproduced data better than $\ln Re_\tau$ (Smits *et al.* 2021). Recent measurements of Ono *et al.* (2022) in pipes for Re_τ ranging from 990 to 20 750 are also supportive of the bounded behaviour. The results of CS have been checked against DNS data in the open channel (Yao *et al.* 2022) and compressible channel (Gerolymos & Vallet 2023), indicating possible universality of the bounded behaviour for different flow conditions. Indeed, Hoyas *et al.* (2022) reported that the wall pressure fluctuation in their DNS channel data for Re_τ up to 10^4 might also be bounded. Further, Monkewitz & Nagib (2015) have proposed a bounded perspective on the peak of $\langle uu\rangle^+$ for TBL, but the difference from CS is that the deviation from the asymptotic value of the $\langle uu\rangle^+$ peak, at any finite Reynolds number, is proportional to $1/\ln Re_\tau$; the latter scaling was also considered by Hwang & Eckhardt (2020) and Skouloudis & Hwang (2021) in their analysis of channel flows via a resolvent-based quasilinear approximation.

To discern one among these perspectives as correct beyond doubt, one clearly requires much higher Reynolds numbers than currently covered (or likely to be covered for the foreseeable future) in laboratory experiments or DNS (Nagib, Monkewitz & Sreenivasan 2022). Measurements in the atmospheric boundary layer (Metzger & Klewicki 2001; Metzger, McKeon & Holmes 2007; Zheng & Wang 2016) might be thought of as helpful but various uncertainties characteristic of field measurements prevent a decisive conclusion there also. At the current stage, new theoretical ideas are highly desired to provide additional insights. As noted by Klewicki (2022), the bounded growth, once accepted, would necessitate a reassessment of a number of earlier empirical findings. In this spirit, we obtain an alternative to (1.1) by using the bounded behaviour of (1.2), providing a more complete description of the asymptotic behaviour of wall turbulence (including pressure).

Of interest are the root-mean-square (r.m.s.) profiles of various fluctuating quantities, which depend on both the Reynolds number and the distance from the wall. The present procedure consists of the following steps.

(i) We first show that the Re_τ dependence in the wall-normal variation disappears in the inner region when peak values are used for normalization. This observation presents a good candidate for the inner expansion of r.m.s. profiles.

(ii) We develop a matching procedure between the inner and outer regions, and show that it yields an outer defect law of the type

$$\phi(y^*) = \alpha_\phi - \beta_\phi y^{*1/4}. \tag{1.3}$$

Here, ϕ represents not only $\langle uu\rangle^+$ and $\langle ww\rangle^+$ but also the r.m.s. of pressure fluctuation p'^+ (the superscript prime denotes the r.m.s. throughout the paper); α_ϕ and β_ϕ are constants independent of Re_τ and y^*. The result (1.3) was first presented in Chen & Sreenivasan (2022*b*), and later found by Monkewitz (2023) independently. We may rewrite (1.3) as

$$\phi(y^*)/\phi_p(Re_\tau) \to (\alpha_\phi/\phi_\infty) - (\beta_\phi/\phi_\infty) y^{*1/4}, \tag{1.4}$$

where ϕ_∞, the limiting value of ϕ_p as $Re_\tau \to \infty$, is independent of Re_τ within the framework of CS. This means that the normalization by peak values is asymptotically the same as normalization by wall variables (modulo the constants ϕ_∞). In contrast, this would not be the case if (1.1) were true, since ϕ_p diverges for increasing Re_τ.

(iii) Finally, we make extensive comparisons with the data. The result (1.3) advances (1.2) to a description of wall-normal profiles of $\langle uu\rangle^+$, $\langle ww\rangle^+$ and p'^+. While (1.2) for the peak scaling is invoked to obtain (1.3), (1.1) could be obtained similarly if a $\ln Re_\tau$ scaling for the peak value is used instead. In this sense, matching in itself cannot preclude (1.1) or (1.3), and hence empirical evidence is much needed.

To verify (1.3), DNS data sets are collected for those with a clear Re_τ trend for $\langle uu\rangle^+$, $\langle ww\rangle^+$ and p'^+, all publicly available. In particular, we use the DNS on channels by Lee & Moser (2015) for Re_τ from 550 to 5200, on pipes by Pirozzoli *et al.* (2021) for Re_τ from 500 to 6000, and on TBLs by Schlatter *et al.* (2009, 2010) for Re_τ from 490 to 1270. Higher Re_τ data in the literature (Sillero, Jimenez & Moser 2013; Hoyas *et al.* 2022) are also included for comparison. For experiments, we select $\langle uu\rangle^+$ data from the Princeton pipe by Hultmark *et al.* (2012) for Re_τ from 5411 to 98 187, from the Princeton TBLs by Vallikivi, Ganapathisubramani & Smits (2015) for Re_τ from 4635 to 25 062, and from the Melbourne TBLs by Samie *et al.* (2018) for Re_τ from 6000 to 20 000. Channel experiments are not collected here because of their limited Re_τ variation covered by the DNS of Lee & Moser (2015). Note that the data uncertainty, especially concerning the probe resolution in experiments and grid resolution in the DNS, are not addressed in this paper (see CS for a brief discussion). We do wish to reiterate, however, that there is much need for better-resolved data.

The paper is organized as follows. Section 2 presents data collapse for the inner flow region, which leads to the uniform expansion scheme presented there. Section 3 begins with the verification of outer similarity, followed by the derivation of the defect decay, using comprehensive data comparisons. Section 4 is devoted to a discussion of the geometry effect. A perspective and summary of the results are given in § 5.

2. The Re_τ-scaling for the near-wall region

A general framework for an asymptotic expansion for $\langle uu\rangle^+$, $\langle ww\rangle^+$ and p'^+, represented by ϕ, can be written as (Spalart & Abe 2021; Monkewitz 2022)

$$\phi(y^+, Re_\tau) = f_0(y^+) + f_1(y^+)g(Re_\tau) + f_2(y^+)g^2(Re_\tau) + \text{h.o.t.}, \tag{2.1}$$

where g is the gauge function of Re_τ; f_0, f_1 and f_2 (as well as f introduced below in (2.2)) are general functions depending merely on the wall-normal distance y^+, and h.o.t. indicates high-order terms. For the streamwise mean velocity $\phi = U^+$, a first-order truncation of (2.1) is fairly accurate near the wall. In the rest of this section, we first show data collapse of $\langle uu\rangle^+$, $\langle ww\rangle^+$ and p'^+ after normalization by their corresponding peak values, and then summarize a common expansion for these quantities, which is actually a second-order truncation of (2.1); we pick up the connection to (2.1) in § 2.2.

2.1. *Data collapse near the wall*

Figure 1 shows the profiles of $\langle uu\rangle^+$, for the channel (figure 1*a*,*b*), the pipe (figure 1*c*,*d*) and the TBL (figure 1*e*,*f*). While figure 1*a*,*c*,*e* displays marked Re_τ variations, figure 1*b*,*d*,*f* illustrates excellent data collapse after normalization by peak values; that is

$$\langle uu\rangle^+(y^+, Re_\tau) = \langle uu\rangle_p^+(Re_\tau) f(y^+). \tag{2.2}$$

Note that according to CS, the peak location is an invariant at $y_p^+ \approx 15$. This is generally accepted as correct (at least since Sreenivasan (1989)), see Smits *et al.* (2021). On the other hand, Pirozzoli *et al.* (2021) commented that the invariant peak location is violated by their pipe data, which show that y_p^+ slightly increases from 14.28 at $Re_\tau \approx 500$ to 15.14 at $Re_\tau = 6000$. Nevertheless, using finer near-wall resolutions than in Pirozzoli *et al.* (2021), Yao *et al.* (2023) found no such variation of y_p^+ with Re_τ ($y_p^+ = 15.07, 15.03, 15.50$ for $Re_\tau = 180, 2000, 5000$, respectively). This small variation is typically found by others as well (Moser, Kim & Mansour 1999; Jimenez *et al.* 2010; Chin *et al.* 2014) but it is non-systematic, possibly owing to secondary reasons such as the grid and probe resolutions.

As for (2.2), data collapse for the spanwise velocity fluctuation is achieved via

$$\langle ww\rangle^+(y^+, Re_\tau) = \langle ww\rangle_p^+(Re_\tau) h(y^+), \tag{2.3}$$

where $\langle ww\rangle_p^+$ is the peak value, and h is a y^+-dependent function. As shown in figure 2, different Re_τ curves are in close agreement with each other, with the self-preserving range from the wall to the peak (at $y^+ \approx 45$) or beyond. We note a marginal Re_τ dependence on this peak location; it is hard to tell whether they arise from numerical uncertainty or physical modulation by outer flow structures. Since this variation is marginal, we shall not consider this any further.

Coming now to pressure fluctuations, figure 3(*a*,*c*,*e*) shows Re_τ dependence of p'^+. The best collapse is obtained by plotting $p_p'^+ - p'^+$, as shown in figure 3(*b*,*d*,*f*). On this basis, we may write

$$p'^+(y^+, Re_\tau) = p_p'^+(Re_\tau) - j(y^+), \tag{2.4}$$

where j is (in general) a y^+-dependent function. The collapse extends from the wall to the peak (at $y^+ \approx 30$), with $p_p'^+ - p_w'^+$ a constant around 0.4. This constancy inspires us to postulate (2.4). Instead, if one plots $p'^+/p_p'^+$, data would not collapse (not shown here).

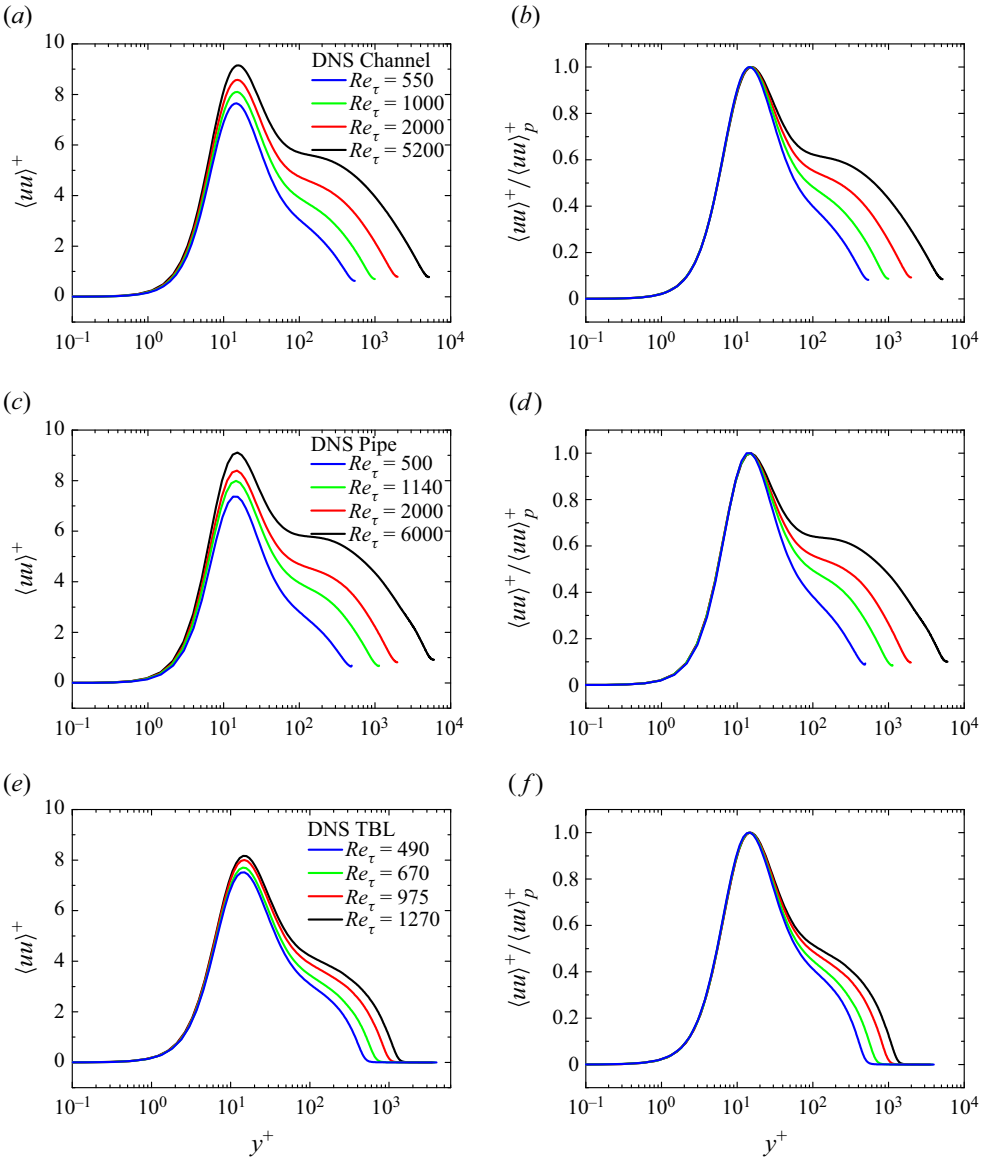

Figure 1. Wall-normal dependence of streamwise velocity fluctuation scaled in viscous units (abscissa in logarithmic scale) for a series of Re_τs in (*a*,*b*) channels, (*c*,*d*) pipes and (*e*,*f*) TBL flows. (*a*,*c*,*e*) Here $\langle uu \rangle^+$ versus y^+. (*b*,*d*,*f*) Here $\langle uu \rangle^+$ normalized by its (inner) peak value $\langle uu \rangle_p^+$, showing very good collapse. Coloured lines indicate DNS data at different Re_τs marked in the figure legends, for channels by Lee & Moser (2015), for pipes by Pirozzoli *et al.* (2021) and for TBLs by Schlatter *et al.* (2009, 2010).

The reason is clear from (2.4), i.e. $p'^+/p_p'^+ = 1 - j(y^+)/p_p'^+(Re_\tau)$: an increasing $p_p'^+$ with Re_τ would eventually spoil the data collapse of $p'^+/p_p'^+$. That is the reason why (2.2) or (2.3) is not applied to p'^+. Note that Panton *et al.* (2017) attempted another data collapse by using $\langle pp \rangle_w^+ - \langle pp \rangle^+$, but it is not as satisfactory as (2.4) in figure 3, as also discussed later in § 3.

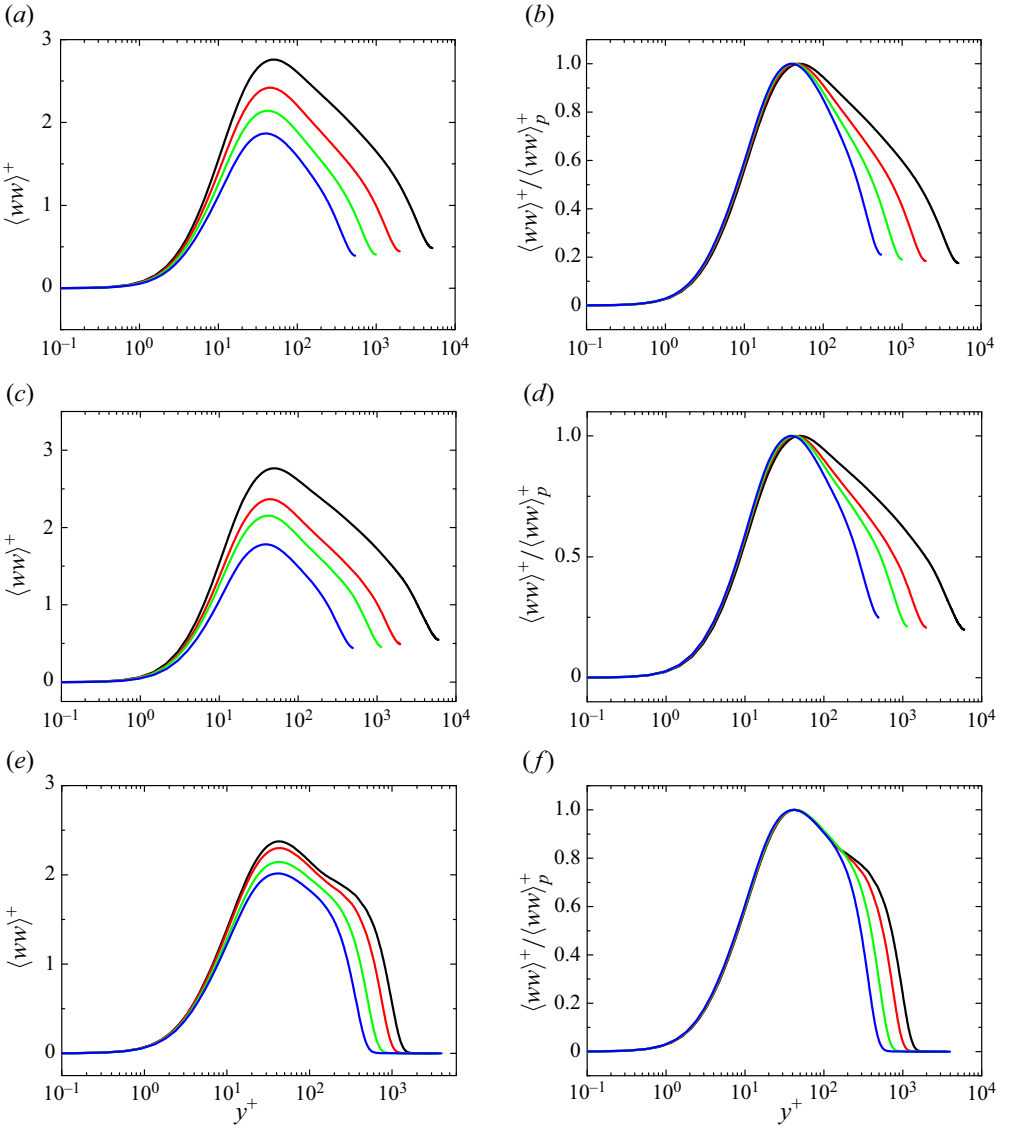

Figure 2. The same plots as in figure 1 but for the spanwise velocity fluctuations: (*a*,*b*) channels, (*c*,*d*) pipes and (*e*,*f*) TBLs; (*a*,*c*,*e*) $\langle ww\rangle^+$, (*b*,*d*,*f*) $\langle ww\rangle^+/\langle ww\rangle_p^+$ versus y^+. Lines represent the same DNS data as in figure 1.

2.2. *Summary for the near-wall scaling*

The above comparisons demonstrate that the Re_τ and y^+ dependencies could be decoupled after a proper normalization by peak values. Recalling (1.2) for the Re_τ-scaling of the peak values and substituting it for $\langle uu\rangle_p^+$, $\langle ww\rangle_p^+$ and $p_p'^+$ into (2.2), (2.3) and (2.4), respectively, one has a uniform expansion, as reinforced for $\langle uu\rangle^+$ also by Monkewitz (2022), i.e.

$$\phi(y^+) = \phi_0(y^+) + \phi_1(y^+)/Re_\tau^{1/4}, \tag{2.5}$$

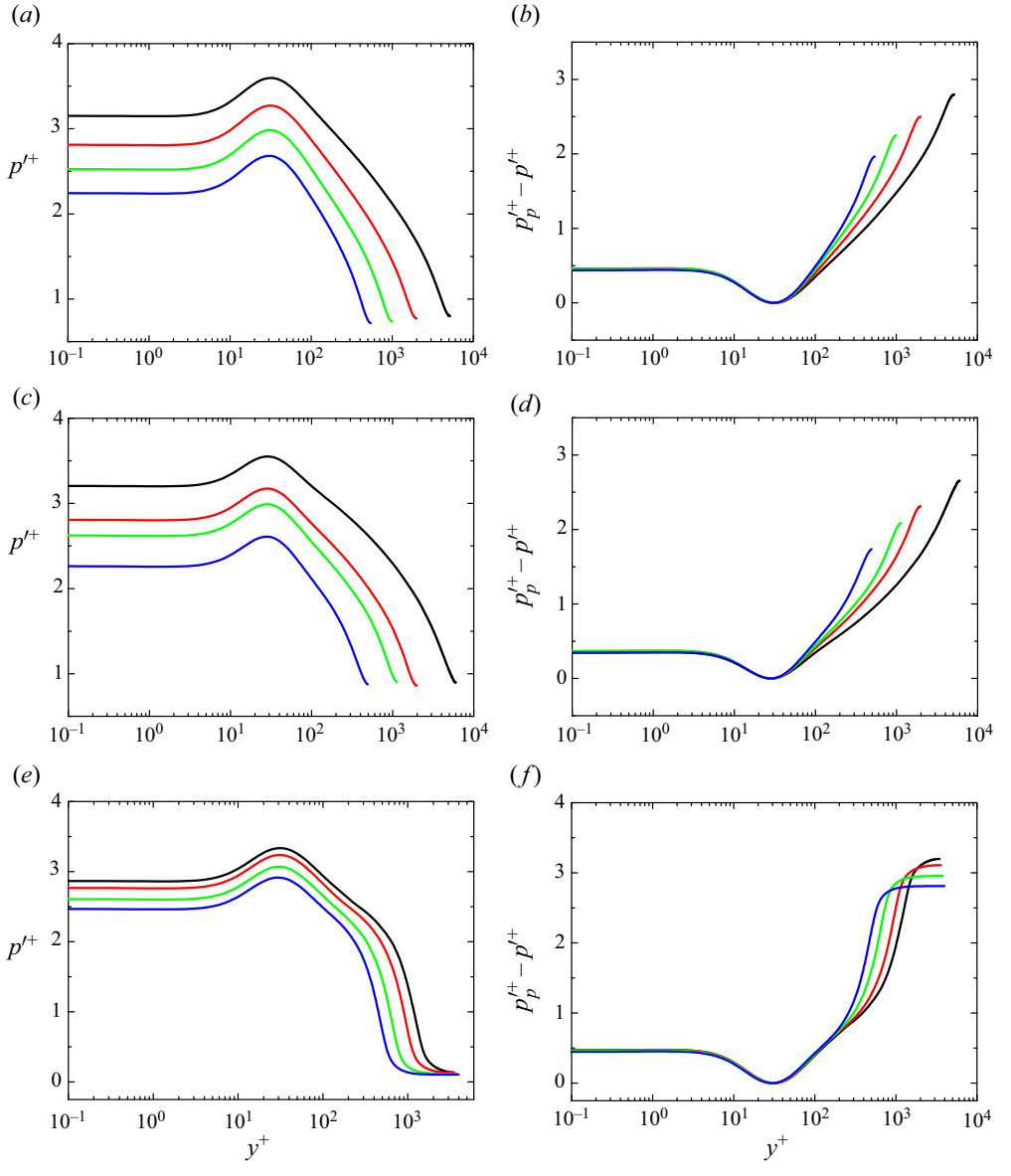

Figure 3. Wall-normal dependence for the r.m.s. of pressure fluctuation $p'^+ = \langle pp\rangle^{+1/2}$ in (a,b) channels, (c,d) pipes and (e,f) TBL flows: (a,c,e) p'^+; (b,d,f) $p_p'^+ - p'^+$ versus y^+. Lines are the same DNS data as in figure 1.

where $\phi_0(y^+) = \phi_\infty f(y^+)$ and $\phi_1(y^+) = -c_{\phi,\infty} f(y^+)$ for u; $\phi_0(y^+) = \phi_\infty h(y^+)$ and $\phi_1(y^+) = -c_{\phi,\infty} h(y^+)$ for w; $\phi_0(y^+) = \phi_\infty - j(y^+)$ and $\phi_1(y^+) = -c_{\phi,\infty}$ for pressure fluctuations.

Note that (2.5) is a specific case of

$$\phi(y^+, Re_\tau) = f_0(y^+) + f_1(y^+) g(Re_\tau), \tag{2.6}$$

which is a second-order truncation of (2.1), considered also by Spalart & Abe (2021) and Monkewitz (2022). If $f_0 = 0$, (2.6) reduces to

$$\phi(y^+, Re_\tau) = f_1(y^+) g(Re_\tau), \tag{2.7}$$

which is the scaling proposed by Smits *et al.* (2021) for $\langle uu\rangle^+$ with $g(Re_\tau) = \epsilon^+_{x-w}$ (streamwise wall dissipation). However, Smits *et al.* (2021) found that their proposal did not work as well for $\langle ww\rangle^+$, which they speculated was due to different superposition and modulation enforced by outer flow structures. Here, we show that replacing wall dissipation by peak value, i.e. $g = \phi_p$, (2.7) applies for both $\langle uu\rangle^+$ and $\langle ww\rangle^+$. Even so, (2.7) is not proper for pressure due to a constancy $p'^+_p - p'^+_w$ as explained earlier. The non-zero f_0 needed in (2.6) has been missed in the past.

Finally, we recall that from (2.6), Monkewitz (2022) developed a composite model for $\langle uu\rangle^+$, which shows that $g = Re_\tau^{-1/4}$ yields a better data description than the alternative $g = \ln Re_\tau$ considered by Smits *et al.* (2021). The gauge function $g = Re_\tau^{-1/4}$ in (2.6) restores wall scaling for asymptotically high Re_τ; we will use it below to derive an outer decay profile, which has not been achieved before.

3. The Re_τ-scaling for the outer region and the defect law for fluctuations

Similar to (2.1) for the inner region, an asymptotic expansion for the outer flow reads

$$\phi(y^*, Re_\tau) = F_0(y^*) + F_1(y^*)G(Re_\tau) + F_2(y^*)G^2(Re_\tau) + \text{h.o.t.}, \tag{3.1}$$

where $y^* = y^+/Re_\tau$ is the outer unit; F_0, F_1 and F_2 are general functions depending on y^*, and $G(Re_\tau)$ is the gauge function. In analogy to law of the wall, the outer flow similarity corresponds to the first-order truncation in (3.1), i.e.

$$\phi(y^*, Re_\tau) = F_0(y^*). \tag{3.2}$$

When we take $\phi = U^+_e - U^+$, the resulting equation for the mean velocity is known as the velocity defect law. Here, the subscript e indicates the value at $y^* = 1$, i.e. the centreline for channel and pipe flows, and the boundary layer edge for TBL. This law has been explored extensively in the literature – see Nagib, Chauhan & Monkewitz (2007) and She, Chen & Hussain (2017) for recent efforts. We shall now develop the equation for the fluctuating quantities.

An assessment of outer similarity for the three fluctuation profiles is shown in figure 4, with figure 4(*a–c*) for the channel, figure 4(*d–f*) for the pipe and figure 4(*g–i*) for the TBL. It is particularly remarkable that the pressure fluctuation displays an excellent data collapse from $y^* = 0.1$ to $y^* = 1$. In the same flow region, the spanwise velocity variance data also collapse well, with a deviation of the order of 0.1 (scaled on u_τ^2). For streamwise velocity, the outer similarity holds better towards the outer edge though discernible Re_τ dependence exists towards small Re_τ. For $Re_\tau > 1000$, the streamwise variance profiles collapse together closely (figures 5 and 6), thus supporting the outer similarity of fluctuations for high Re_τ.

3.1. *Matching for the defect law for fluctuations*

Based on the above inner expansion and outer similarity, we now develop a matching procedure to derive the analytical form in the intermediate zone. One may invoke the derivation of Millikan (1938) for the log law in the mean velocity distribution, which has been extended for $\langle uu\rangle^+$ by Hultmark (2012) and for $\langle pp\rangle^+$ by Panton *et al.* (2017). Nevertheless, different orders of matching would lead to different scaling proposals, and here we present a short account of matching to obtain the defect law for fluctuations.

As a starting point, we note an exact matching between the inner and outer flows for the total stress in channels or pipes. That is, $\tau^+(y^+, Re_\tau) = 1 - y^+/Re_\tau$, which can be

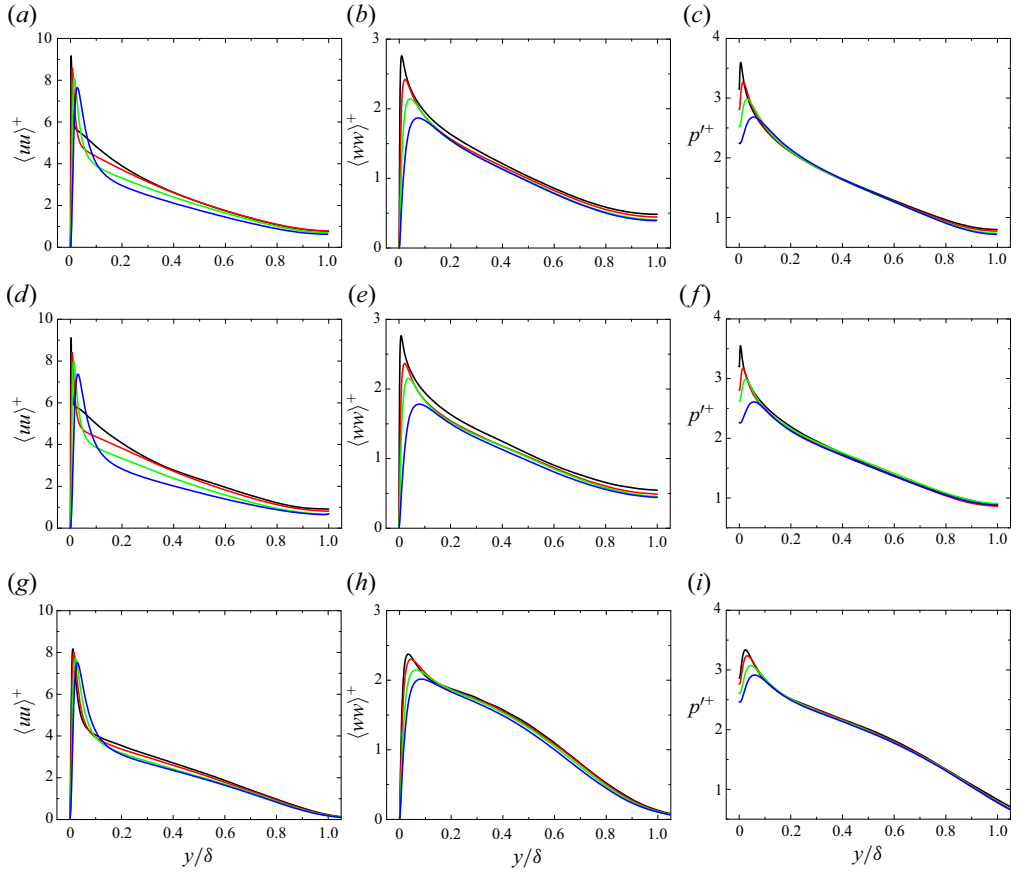

Figure 4. Wall-normal dependence of turbulence fluctuations in outer length unit $y^* = y/\delta$ (the abscissa in linear scale): (*a–c*) channels, (*d–f*) pipes and (*g–i*) TBLs; (*a,d,g*) $\langle uu\rangle^+$; (*b,e,h*) $\langle ww\rangle^+$; (*c,f,i*) p'^+. Lines are the same DNS data as in figure 1.

rewritten as $\tau^+(y^*, Re_\tau) = 1 - y^*$. The first version of $\tau^+(y^+, Re_\tau)$ corresponds to the two-term inner expansion of (2.6) with $\phi = \tau^+, f_0(y^+) = 1, f_1(y^+) = y^+$ and $g = Re_\tau^{-1}$; the second version of $\tau^+(y^*, Re_\tau)$ corresponds to the one-term expansion in (3.1), or to the outer similarity in (3.2) with $\phi = \tau^+$ and $F_0(y^*) = 1 - y^*$. Thus, the total stress satisfies a straightforward matching between (2.6) and (3.2), i.e. $f_0(y^+) + f_1(y^+)g(Re_\tau) = F_0(y^*)$, valid for the entire flow, quite unlike Millikan's matching analysis that requires $1/Re_\tau \ll y^* \ll 1$ (or $1 \ll y^+ \ll Re_\tau$) and dictates a term-by-term balance.

Therefore, we match (2.6) directly with (3.2), i.e. $\phi(y^+, Re_\tau) = F_0(y^*)$, and obtain

$$\begin{aligned}\phi(y^+, Re_\tau) &= f_0(y^+) + f_1(y^+)/Re_\tau^{1/4} \\ &= f_0(y^+) + h_1(y^+)y^{*1/4} \\ &= F_0(y^*)\end{aligned} \tag{3.3}$$

(where $g = Re_\tau^{-1/4}$ is used and $h_1(y^+) = f_1(y^+)/y^{+1/4}$). Note that $f_0 = \phi_0$ and $h_1 = \phi_1/y^{+1/4}$ as the wall is approached, so that (3.3) approaches (2.5), but f_0 and h_1 towards the outer region are to be determined. At this stage, as $F_0(y^*)$ in (3.3) depends only on y^*,

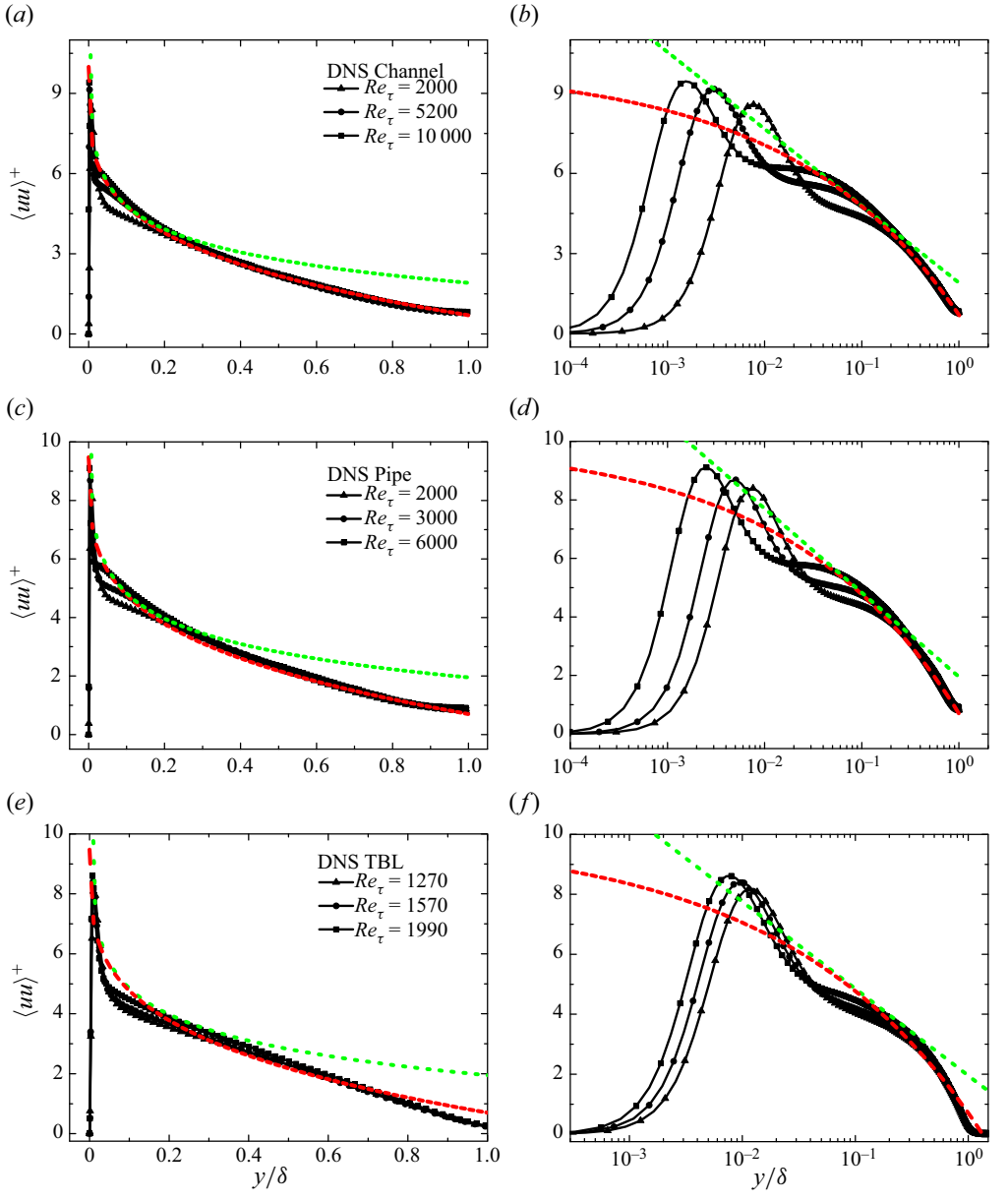

Figure 5. Variance of streamwise velocity fluctuation of DNS data at high Re_τ. Channel data in (*a*,*b*) are $Re_\tau = 2000$, 5200 from Lee & Moser (2015), $Re_\tau = 10^4$ from Hoyas *et al.* (2022). Pipe data in (*c*,*d*) from Pirozzoli *et al.* (2021). Panels (*e*,*f*) for TBL, $Re_\tau = 1270$ from Schlatter & Örlü (2010), $Re_\tau = 1570$, 1990 from Sillero *et al.* (2013). Here (*a*,*c*,*e*) is for abscissa in linear and (*b*,*d*,*f*) in logarithmic outer units $y^* = y/\delta$, to highlight wall-normal distances close to the wall. Dotted (green) line in (*a*,*b*) indicates $1.61 - 1.25 \ln y^*$ by Hultmark *et al.* (2012); $2.2 - 1.26 \ln y^*$ in (*c*,*d*) by Marusic *et al.* (2013) and $1.95 - 1.26 \ln y^*$ in (*e*,*f*) by Samie *et al.* (2018). Dashed (red) lines indicate the present relation (1.3), i.e. $10 - 9.3 y^{*1/4}$, the same for all the flows here.

Quantity ϕ	$\alpha_\phi^{(CH)}$	$\alpha_\phi^{(Pipe)}$	$\alpha_\phi^{(TBL)}$	$\beta_\phi^{(CH)}$	$\beta_\phi^{(Pipe)}$	$\beta_\phi^{(TBL)}$
$\langle uu\rangle^+$	10	10	10	9.3	9.3	9.3
$\langle ww\rangle^+$	3.9	3.9	3.6	3.45	3.45	2.6
p'^+	4.84	4.6	4.65	4.1	3.7	3.15

Table 1. Parameters in (1.3), for different fluctuations. Superscripts 'CH', 'Pipe' and 'TBL' represent channel, pipe and boundary layer flows, respectively. Note that both α_ϕ and β_ϕ vary only modestly among different flows, implying that essentially the same mechanisms applies for all flows. Moreover, β_ϕ is quite close to α_ϕ, as ϕ at the boundary layer edge $y^* = 1$ is fairly small.

we have $\partial F_0(y^*)/\partial y^+ = 0$ in (3.3), and hence

$$f_0(y^+) = c_0, \tag{3.4a}$$

$$h_1(y^+) = c_1, \tag{3.4b}$$

where c_0 and c_1 are constants independent of y^*, y^+ and Re_τ, but may depend on the variable ϕ. Denoting $c_0 = \alpha_\phi$ and $c_1 = -\beta_\phi$, we obtain (1.3) from (3.3) and (3.4). It is readily verified that (1.3) matches (3.2) in the outer region and (2.6) in the inner, hence offers a common description connecting the two.

In the above procedure, we have assumed that the two-term expansion $f_0(y^+) + f_1(y^+)g(Re_\tau)$ extends to the outer flow, so that it matches with $F_0(y^*)$ and satisfies the outer similarity as well. As explained above, the procedure works exactly for the total stress in channels and pipes with $g = Re_\tau^{-1}$.

3.2. *Comparison with the data*

Figures 5–8 show comparisons of data with (1.1) and (1.3) for $\langle uu\rangle^+$, $\langle ww\rangle^+$ and p'^+, respectively. Table 1 collects all the parameters for the three profiles, arising from these fits to the data, which we now discuss.

Similar to figures 1–3, figures 5(*a*,*b*), 6(*a*,*b*), 7(*a*,*b*) and 8(*a*,*b*) are for channel, figures 5(*c*,*d*), 6(*c*,*d*), 7(*c*,*d*) and 8(*c*,*d*) for pipe and figures 5(*e*,*f*), 6(*e*,*f*), 7(*e*,*f*) and 8(*e*,*f*) for boundary layers; for figures 5(*a*,*c*,*e*), 6(*a*,*c*,*e*), 7(*a*,*c*,*e*) and 8(*a*,*c*,*e*) the abscissa are in linear units while for figures 5(*b*,*d*,*f*), 6(*b*,*d*,*f*), 7(*b*,*d*,*f*) and 8(*b*,*d*,*f*), logarithmic units are used. A difference from figures 1–3 is that the data in figures 5–8 are denoted by black symbols, so that (1.1) and (1.3) are better marked to guide the eye.

Particularly for $\langle uu\rangle^+$, to avoid distractions by data scatter at small Re_τ, we collect in figure 5 only high Re_τ profiles from DNS, namely, Re_τ from 2000 to 10^4 for channel; 2000 to 6000 for pipe; and 1270 to 1990 for TBL. Compared with figure 4(*a*,*d*,*g*), it is clear in figure 5(*a*,*c*,*e*) that all high Re_τ profiles collapse on each other in the flow range $0.1 \lesssim y^* \lesssim 1$, thus bearing witness to outer similarity. This is confirmed again by experimental data in figure 6 corresponding to higher Re_τ.

Note that the logarithmic behaviour advanced in the literature (Hultmark *et al.* 2012; Marusic *et al.* 2013; Samie *et al.* 2018) is indicated by a green dotted line. Although it characterizes data in the region from $0.1 \lesssim y^* \lesssim 0.3$, the value of the intercept B_ϕ needs to be adjusted for the three flows from 1.61 to 2.2, while A_ϕ holds constant around 1.26. In contrast, the red dashed line represents (1.3) with the same $\alpha_\phi = 10$ and $\beta_\phi = 9.3$, which reproduces data well for channel, pipe and TBL flows, covering not only the logarithmic range (*vis-à-vis* the mean flow) but also the so-called wake region, almost all the way to the centreline of channel and pipe flows.

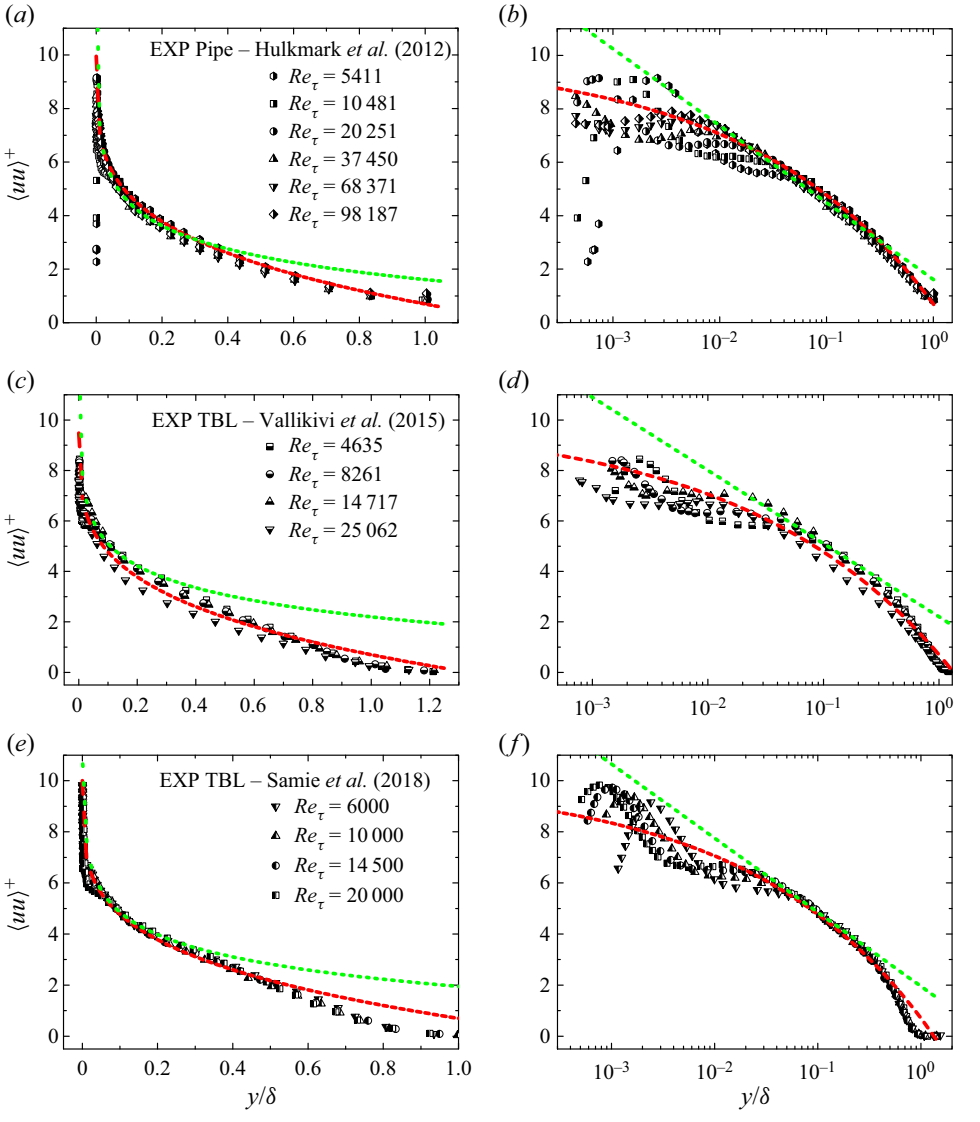

Figure 6. Variance of streamwise velocity fluctuation in high Re_τ experiments. Data in (*a*,*b*) from Princeton pipe (Hultmark *et al.* 2012), (*c*,*d*) from Princeton TBL (Vallikivi *et al.* 2015) and (*e*,*f*) from Melbourne TBL (Samie *et al.* 2018). Dotted (green) line in (*a*,*b*) indicates $1.61 - 1.25 \ln y^*$ by Hultmark *et al.* (2012); $2.2 - 1.26 \ln y^*$ in (*c*,*d*) by Marusic *et al.* (2013) and $1.95 - 1.26 \ln y^*$ in (*e*,*f*) by Samie *et al.* (2018). Dashed (red) lines indicate (1.3), i.e. $10 - 9.3 y^{*1/4}$ in all the panels (here $y^* = y/\delta$).

One may imagine that the data in figure 5 have not reached the asymptotic state and that (1.1) might agree with data better for higher Re_τ. But experimental data from Princeton pipes (Hultmark *et al.* 2012) with Re_τ covering one more decade, e.g. Re_τ from approximately 5000 to 10^5, do not show any improvement of the fit to (1.1) (see figure 6*a*,*b*). A similar observation is also true for the TBL, as shown in figure 6(*c*–*f*).

Likewise, for $\langle ww \rangle^+$ and p'^+, (1.3) extends almost all the way to the centreline of channel and pipe flows. Here, data in figures 7 and 8 are the same DNS groups as in figure 1 and contain those low Re_τ profiles. The agreement with (1.3) is excellent at the

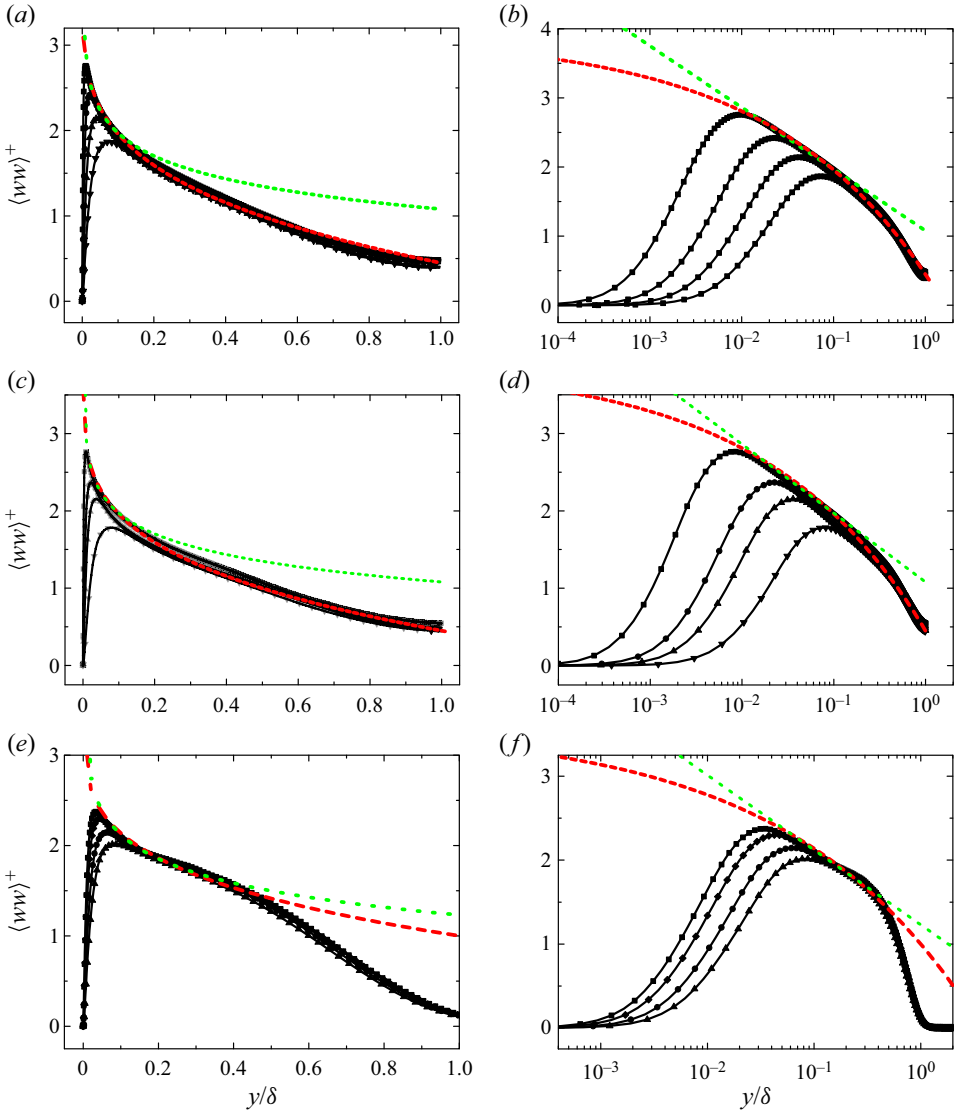

Figure 7. Variance of spanwise velocity fluctuation in channel (*a*,*b*), pipe (*c*,*d*) and TBL (*e*,*f*) flows scaled in outer units $y^* = y/\delta$. Dashed (red) lines indicate the bounded decay (1.3) with parameters in table 1. Dotted (green) lines indicate the logarithmic decay (1.1), i.e. $1.08 - 0.387 \ln y^*$ for channel and pipe, and $1.23 - 0.387 \ln y^*$ for TBL. Symbols with lines are the same DNS data as in figure 1, i.e. channel from Lee & Moser (2015), pipe from Pirozzoli *et al.* (2021), TBL from Schlatter *et al.* (2009, 2010).

smallest $Re_\tau \approx 500$ for channel and pipe, in contrast to the log variation that agrees with data only for $Re_\tau \gtrsim 2000$. Therefore, in both y and Re_τ ranges, (1.3) covers a wider range than (1.1).

Three further points will now be discussed. First, the difference between (1.3) and (1.1) is more vital for asymptotically high Re_τ. For (1.1), an infinitely large of $\phi \propto \ln Re_\tau$ would arise as $y^* \to 0$ and $Re_\tau \to \infty$. In contrast, (1.3) assigns a plateau of $\phi \approx \alpha_\phi$ in the same limit. Such an asymptotic plateau implies that turbulent eddies in the bulk would be in a quasiequilibrium state in the sense that their contribution to ϕ is invariant when y changes.

Note also that according to (1.3), the outer peak of $\langle uu\rangle^+$, if it exists, should be bounded by $\langle uu\rangle^+ \approx 10$. Clarification of such differences of perspectives in the asymptotic state require data at higher Reynolds numbers.

Second, while (1.3) adheres closely with TBL data of Vallikivi *et al.* (2015) up to $y^* = 1$ (figure 6*c*), it is slightly and uniformly higher than the TBL data of Samie *et al.* (2018) for $y^* > 0.6$ (figure 6*e*). This is due to the fact that the former set of data are obtained for flow over a flat plate mounted in the same pipe in which data of Hultmark *et al.* (2012) are measured. Therefore, the data of Vallikivi *et al.* (2015) in its outer wake region resemble the centre behaviour of pipe data by Hultmark *et al.* (2012), both in agreement with (1.3) up to $y^* = 1$. In contrast, TBL data of Samie *et al.* (2018) are measured in the Melbourne wind tunnel with the standard free stream boundary condition, so that a vanishing $\langle uu\rangle^+ \approx 0$ towards the boundary layer edge is observed (figure 6*e*,*f*), which is lower than (1.3). This difference reflects the wake influence on $\langle uu\rangle^+$ in TBL. In fact, the wake influence is much sharper for $\langle ww\rangle^+$ and p'^+ in TBL (figures 7*e* and 8*e*). This issue will be addressed in § 4.2.

The third point is that, for p'^+, the green dotted line in figure 8 represents

$$p'^+(y^*) = \sqrt{B_\phi - A_\phi \ln y^*}, \tag{3.5}$$

which is the square root of (1.1) for pressure variance

$$\langle pp\rangle^+(y^*) = B_\phi - A_\phi \ln y^*. \tag{3.6}$$

This equation is obtained by Panton *et al.* (2017) via an inner–outer matching (i.e. a viscous inner layer overlapping with an inviscid outer layer). It is almost indistinguishable from (1.3) in figure 8. Nevertheless, as shown in figure 9(*a–c*), $\langle pp\rangle_w^+ - \langle pp\rangle^+$ versus y^+ produces no data collapse for $y^+ > 5$. Particularly for the trough located at approximately $y^+ = 30$, the data are markedly lower for increasing Re_τ, thus creating a challenge for the inner–outer matching analysis. To reconcile this challenge, Panton *et al.* (2017) introduced two logarithmic slopes, i.e. $A^{CP} = 2.56$ for the common part of presumed log profile in the overlap layer, and another $A^w = 2.24$ for the Re_τ variation of the wall pressure. Following this fix, one can estimate

$$\langle pp\rangle_p^+ - \langle pp\rangle_w^+ \propto (A^{CP} - A^w)\ln Re_\tau \approx 0.32 \ln Re_\tau, \tag{3.7}$$

which would break the wall scaling completely.

As a comparison, figure 3(*b*,*d*,*f*) show that data of $p'^+_w - p'^+$ collapsed well up to the trough, better than $\langle pp\rangle_w^+ - \langle pp\rangle^+$ in figure 9(*a–c*). Moreover, via the bounding relation $p'^+_w \approx 4.4 - 10.5/Re_\tau^{1/4}$ and $p'^+_p \approx 4.84 - 10.5/Re_\tau^{1/4}$ given in CS, we have

$$\langle pp\rangle_p^+ - \langle pp\rangle_w^+ = p'^{+2}_p - p'^{+2}_w \approx 4.07 - 9.24/Re_\tau^{1/4}, \tag{3.8}$$

which depicts data satisfactorily over a wider Re_τ range than (3.7) in figure 9(*d*).

Finally, to evaluate the goodness of the theoretical fits with the data, taking the channel at $Re_\tau = 5200$ (Lee & Moser 2015) for example, we have calculated the variance of difference between DNS data (ϕ_{Data}) and theoretical predictions (ϕ_{Eq}), i.e. $\sigma^2 = \sum_{0.1\le y_i^*\le 1}[\phi_{Data}(y_i^*) - \phi_{Eq}(y_i^*)]^2/N$ where N is the total number of data points in the range from $y^* = 0.1$ to $y^* = 1$. For (1.3), σ^2 is 0.007 for $\langle uu\rangle^+$, 0.002 for $\langle ww\rangle^+$ and 0.002 for p'^+; while for (1.1), σ^2 is 0.26, 0.14 and 0.004 for $\langle uu\rangle^+$, $\langle ww\rangle^+$ and p'^+, respectively. The larger σ^2 of (1.1) for $\langle uu\rangle^+$ and $\langle ww\rangle^+$ is not surprising because of their deviation from data towards the centreline. But we should remember that (1.1) is derived for asymptotically high Re_τ and is not supposed to depict the data behaviour towards

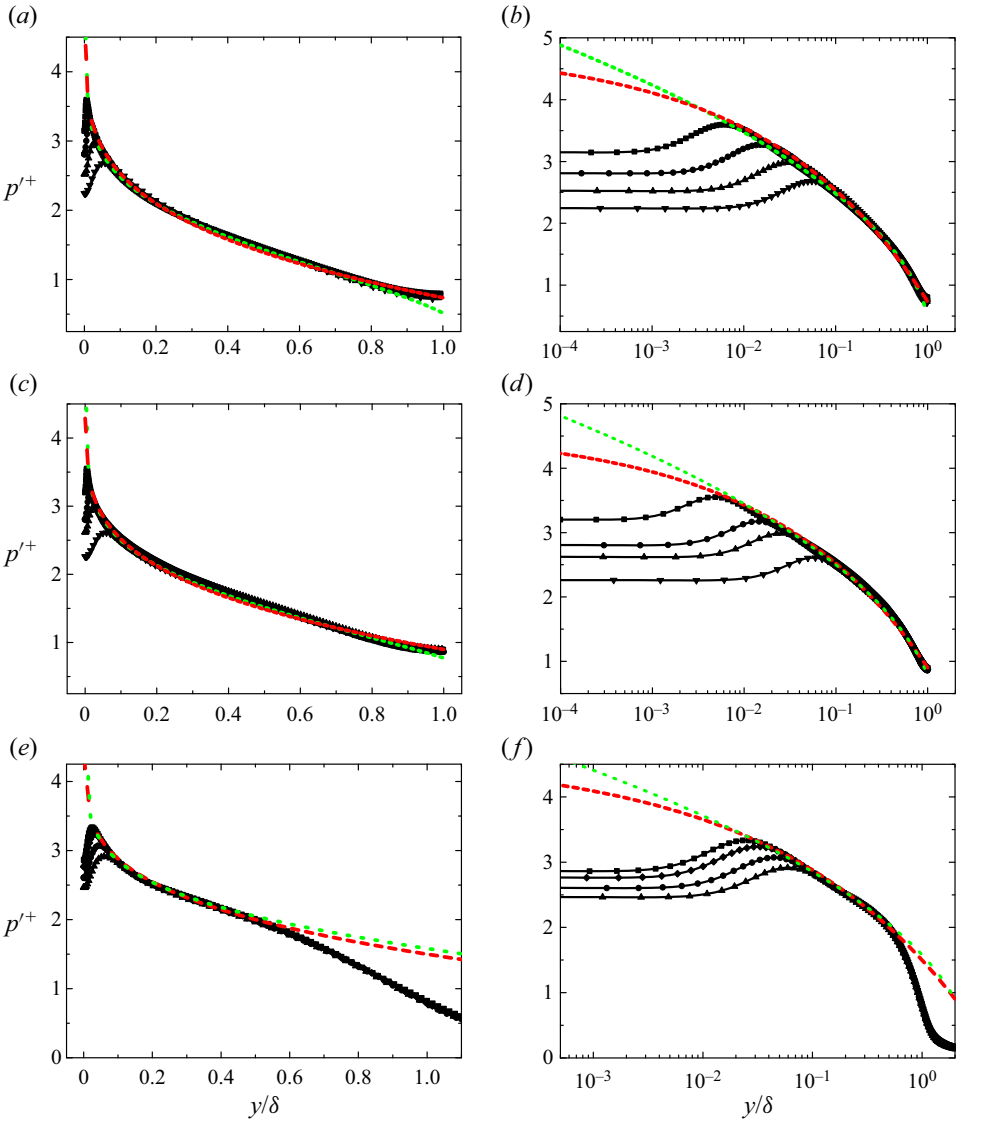

Figure 8. The r.m.s. of pressure fluctuation in channel (*a*,*b*), pipe (*c*,*d*) and TBL (*e*,*f*) flows scaled in the outer unit $y^* = y/\delta$. Dashed (red) lines indicate the bounded decay (1.3) with parameters in table 1. Dotted (green) lines indicate the logarithmic decay in (3.5), i.e. $\sqrt{0.27 - 2.56 \ln y^*}$ for channel, $\sqrt{0.6 - 2.45 \ln y^*}$ for pipe and $\sqrt{2.5 - 2.45 \ln y^*}$ for TBL. Symbols with lines are the same DNS data as in figure 7.

$y^* = 1$. In this sense, $1/Re_\tau \ll y^* \ll 1$ might be better for the competition between the two proposals, but that would lose sight of the advantage that (1.3) covers a wider outer domain.

3.3. *Brief critique of the matching arguments*

Two further points will be considered here. Despite the agreement with the data, one should note that, according to (1.3), $\partial\phi/\partial y^* = -\beta_\phi/4$ at $y^* = 1$, which is against the mirror symmetry of $\partial\phi/\partial y^* = 0$ at the centreline of channel and pipe. This indicates that

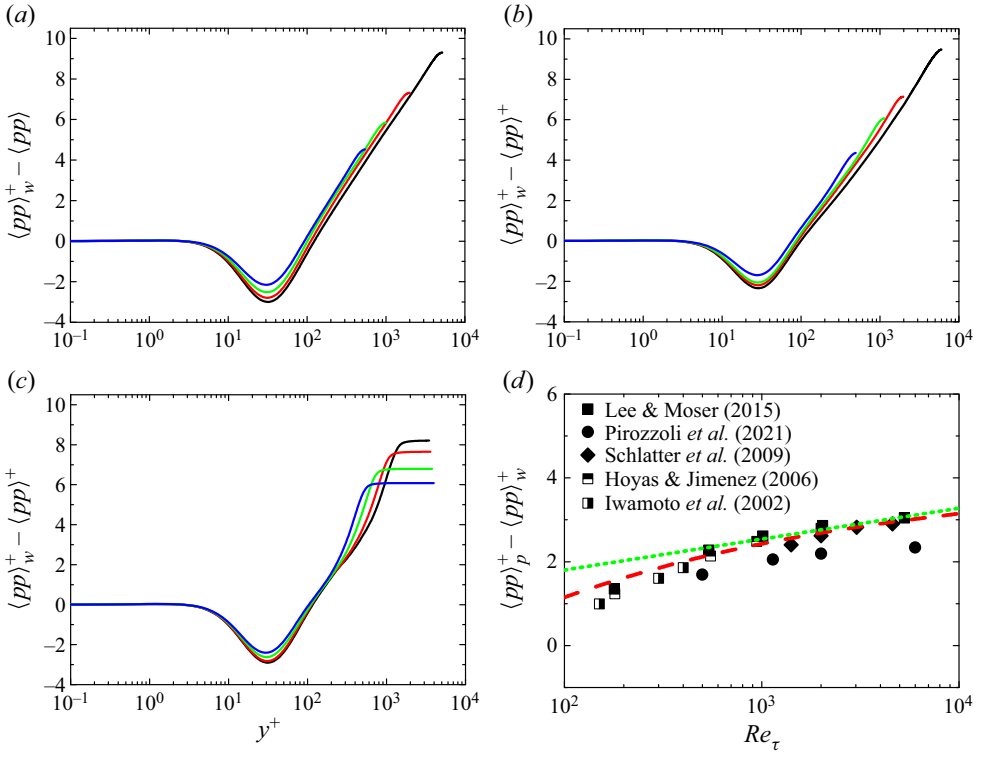

Figure 9. Wall-normal dependence of the variance of pressure fluctuations is shown in the plots of $\langle pp\rangle_w^+ - \langle pp\rangle^+$ versus y^+, where $\langle pp\rangle_w^+$ is the wall-value of $\langle pp\rangle^+$. Lines are the same DNS data as in figure 3: (*a*) channels; (*b*) pipes; (*c*) TBLs. Note that lines depart markedly from each other with increasing Re_τ in the region $y^+ > 5$. (*d*) Difference between the peak and wall values of pressure variance, i.e. $\langle pp\rangle_p^+ - \langle pp\rangle_w^+$, for channel, pipe and TBL flows for a series of Re_τ values. Dotted line (green) indicates the logarithmic growth by (3.7), i.e. $0.32\ln Re_\tau + 0.33$. Dashed line (red) indicates the bounded variation of (3.8) according to CS. Symbols are DNS data, squares for channel (Lee & Moser 2015), circles for pipe (Pirozzoli *et al.* 2021) and diamonds for TBL (Schlatter *et al.* 2009). Note that DNS channel data at $Re_\tau = 150, 300, 400$ of Iwamoto, Suzuki & Kasagi (2002), and $Re_\tau = 180, 550, 944, 2000$ of Hoyas & Jimenez (2006) are also included here.

there is a discrepancy between (1.3) and data towards the centreline, for which a centre core layer or the wake modification is needed, as shown in Monkewitz (2023).

Secondly, a perusal of the fits with data suggests the existence of a gap between the inner peak and the outer data collapse, particularly for $\langle uu\rangle^+$ (figure 1*b*,*d*,*f*). This indicates a modest Re_τ-dependence even after normalization by the peak. This may also be the influence of higher-order terms in (2.1), as explained here by the two-term expansion. From (2.6), we expand $\phi(y^+)/\phi_p(y^+)$ by the parameter $g(Re_\tau)$; that is,

$$\frac{\phi(y^+)}{\phi(y_p^+)} = \frac{f_0(y^+)}{f_0(y_p^+)}\left\{1 + \left[\frac{f_1(y^+)}{f_0(y^+)} - \frac{f_1(y_p^+)}{f_0(y_p^+)}\right] g(Re_\tau) + \cdots\right\}. \tag{3.9}$$

When $f_0(y^+)$ and $f_1(y^+)$ are proportional to each other, one has $f_1(y^+)/f_0(y^+) - f_1(y_p^+)/f_0(y_p^+) = 0$, and hence $\phi(y^+)/\phi(y_p^+)$ from (3.9) is independent of $g(Re_\tau)$. This case corresponds to the data collapse of $\langle uu\rangle^+$ from the wall to the peak. However, when $f_0(y^+)$ and $f_1(y^+)$ are no longer proportional to each other, the gauge function $g(Re_\tau)$ in (3.9) indicates that (3.9) still has Re_τ-dependence, which corresponds to the gap between the

inner peak and the outer approximation (1.3). Therefore, the proportionality or otherwise of $f_0(y^+)$ and $f_1(y^+)$ in (2.6) would determine the data collapse or slight mismatch when plotting via $\phi(y^+)/\phi(y_p^+)$. There is no stipulation here that the ratio of $f_0(y^+)$ to $f_1(y^+)$ is constant in matching (3.3). In fact, according to (3.4), $f_0(y^+)/f_1(y^+) = c_0/(c_1 y^{+1/4})$. Therefore, even if f_0 and f_1 are not proportional to each other, we can still match (2.6) with (3.2) to obtain (3.3).

4. Discussion on the influence of flow geometry

4.1. *Near wall universality*

We focus here on the geometry effects. First, a universal data collapse is summarized by unifying (2.2), (2.3) and (2.4) together, i.e.

$$\frac{\phi(y^+, Re_\tau) - \phi_w(Re_\tau)}{\phi_p(Re_\tau) - \phi_w(Re_\tau)} = f_\phi(y^+), \tag{4.1}$$

where $f_\phi(y^+)$ depends on y^+ and ϕ but is independent of Re_τ. For $\langle uu\rangle^+$, $\phi_w = 0$ so that (4.1) reduces to (2.2); the same is true for $\langle ww\rangle^+$. For p'^+, as $\phi_p - \phi_w$ is a constant independent of Re_τ shown in figure 3, (4.1) reproduces (2.4) with $f_\phi = 1 - j(y^+)/j(0)$.

Moreover, as y^+ moves from the wall to the peak location, it is interesting to check whether $f_\phi(y^+)$ is universal for channel, pipe and TBL flows. This is indeed verified in figure 10(*a–c*), for $\langle uu\rangle^+$, $\langle ww\rangle^+$ and p'^+, respectively. Profiles from these three wall flows collapsed together from the wall to the peak location, which means that Re_τ-dependence and geometry influence are cancelled by the ratio of relative variations composed of ϕ_w and ϕ_p. This is conceivable if the near-wall region is viewed as a self-organized entity, so that superposition and modulation effects enforced by the outer flow structures are characterized to the first order by wall and peak values.

4.2. *Wake modification in TBL*

Note that in figures 7 and 8, $\langle ww\rangle^+$ and p'^+ depart from (1.3) for $y^* \gtrsim 0.5$ in TBL, but the agreement persists all the way to the centreline of channel and pipe flows. Recall the findings by Chen, Hussain & She (2019) that the total shear stress τ^+ and the Reynolds shear stress $\langle -uv\rangle^+$ in the wake of the TBL differ notably from that in channel and pipe flows. The reason for this difference, according to Chen *et al.* (2019), is the non-zero mean momentum transport in the wall-normal direction of TBL, i.e. $V/V_e \propto y^{*3/2}$ (the subscript e indicates the value at the boundary layer edge, as noted earlier), which offers a power law modelling for the V profile in the bulk region. The latter leads to $\langle -uv\rangle^+ \approx \tau^+ \approx 1 - y^{*3/2}$ in TBL, differing from $\langle -uv\rangle^+ = 1 - y^*$ in channel and pipe flows for which $V \equiv 0$.

Once we accept the difference in the $\langle -uv\rangle^+$ behaviour, we may expect a similar wake modification on $\langle ww\rangle^+$ and p'^+ by the non-zero V in TBL; that is,

$$\phi - \phi_e \propto \phi_{uv} - \phi_{uv,e}, \tag{4.2}$$

where ϕ represents $\langle ww\rangle^+$ or p'^+, and ϕ_{uv} represents $\langle -uv\rangle^+$. If so, substituting $\phi_{uv} \approx 1 - y^{*3/2}$ into (4.2) yields

$$\phi(y^*) - \phi_e = c_\phi(\phi_{uv} - \phi_{uv,e}) \approx c_\phi(1 - y^{*3/2}), \tag{4.3}$$

where the proportionality coefficient c_ϕ is independent of y^* but may depend on ϕ.

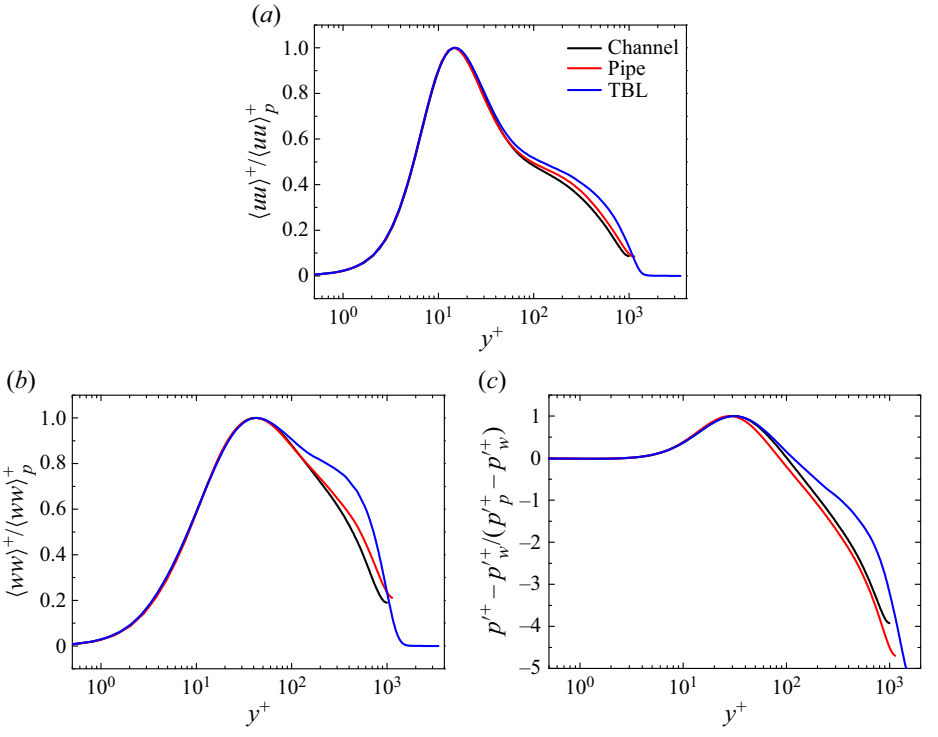

Figure 10. Wall-normal dependence for fluctuations after normalization by the corresponding peaks: (*a*) $\langle uu\rangle^+/\langle uu\rangle_p^+$; (*b*) $\langle ww\rangle^+/\langle ww\rangle_p^+$; (*c*) $(p'^+ - p_w'^+)/(p_p'^+ - p_w'^+)$. Lines are DNS data of channel at $Re_\tau = 1000$ (Lee & Moser 2015), of pipe at $Re_\tau = 1140$ (Pirozzoli *et al.* 2021) and of TBL at $Re_\tau \approx 1270$ (Schlatter *et al.* 2010), all of which collapse closely on each other near the wall.

Verification of (4.3) for TBL is provided in figure 11. The agreement with the data is quite satisfactory for $y^* > 0.2$, and the fitting parameters are $\phi_e = 0$ and $c_\phi = 2.02$ for $\langle ww\rangle^+$, while $\phi_e = 0.8$ and $c_\phi = 1.8$ for p'^+. This model for the wake flow could also be applied to describe $\langle uu\rangle^+$ towards the free stream of the TBL, but the deviation is fairly small as shown in figures 5(*e*) and 6(*e*). Monkewitz & Nagib (2023) have shown a different behaviour of $\langle uu\rangle^+$ and U^+ profiles in the TBL compared with channel and pipe flows using scaling indicator function, which implies different flow physics between external and internal flows.

5. Perspective and conclusions

New methods of analysis and generations of new experiments and simulations have revealed deeper and interesting questions on wall flow dynamics. Previously unthinkable questions, such as the universality of the Kármán constant in the mean flow description (Nagib *et al.* 2017; Monkewitz & Nagib 2023) and the scaling of fluctuations in these flows, as well as the implications of the behaviour of fluctuations for the mean velocity itself, can now be asked, and reasonable answers for them can be attempted. In contrast to the mean velocity, concerted effort to understand the scaling of fluctuations is relatively new. This paper, when taken together with our earlier work (Chen & Sreenivasan 2021, 2022*a*), provides a self-consistent description of fluctuations in streamwise and spanwise velocity, as well as pressure fluctuations. One of the main qualitative conclusions of this work is that

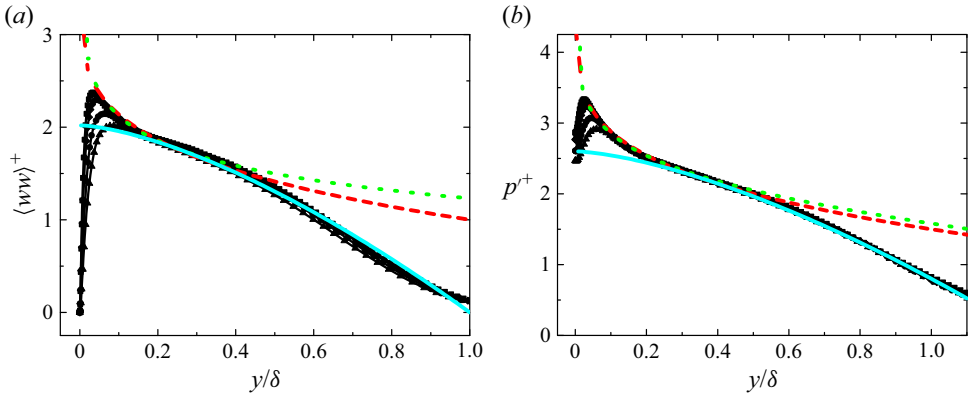

Figure 11. Same plot as figure 7(*e*) for $\langle ww\rangle^+$, and as 8(*e*) for p'^+, with newly added solid (cyan) lines (4.3) for wake modification in TBL. That is, $\langle ww\rangle^+ = 2.02(1 - y^{*3/2})$ in (*a*) and $p'^+ = 0.8 + 1.8(1 - y^{*3/2})$ in (*b*).

wall-normalized fluctuations are bounded even when $Re_\tau \to \infty$, thus restoring the validity of the standard law of the wall. The alternative scenario of attached-eddy hypothesis and its consequences lead to a different conclusion.

We should reiterate that there exists no rigorous proof of either (1.1) or (1.3). The first step in establishing such a proof might be to justify the boundedness or otherwise of the peak values. An expansion analysis like that of Monkewitz & Nagib (2015) is highly desired, but how to choose a correct expansion parameter from first principles is currently unclear. Similarly, the quasilinear approximation by Hwang & Eckhardt (2020) is of also interest, as such an approach could reveal with much less computation the asymptotic feature of the Navier–Stokes equations as $Re_\tau \to \infty$. There are significant issues for future study.

Aiming for an asymptotic description of fluctuations in canonical wall flows, we have obtained several new results, summarized as follows. First, excellent data collapse is achieved for the near-wall r.m.s. profiles of streamwise and spanwise velocity fluctuations ($\langle uu\rangle^+$ and $\langle ww\rangle^+$) as well as pressure fluctuations (p'^+). Their spatial variations and the Reynolds number dependence are decoupled via the normalization through peak values. With the defect law for the peaks given in CS, a universal near-wall expansion (2.6) is obtained with the specific gauge function $g = Re_\tau^{-1/4}$.

Moreover, a defect decay (1.3) is derived by matching (2.6) with the outer similarity (3.2). Compared with the log profile by Townsend's attached-eddy hypothesis, it is shown that (1.3) reproduces the data better, not only over a wider Re_τ domain but also in a larger flow region. As indicated by (1.3), there would appear an asymptotic plateau as $y^* \to 0$ and $Re_\tau \to \infty$, which implies a quasiequilibrium state with contributions to fluctuations coming from all associated eddies that are invariant as wall-normal position changes. If so, the intriguing outer peak of streamwise fluctuation, if one exists, would be bounded by $\langle uu\rangle^+ \approx 10$.

Finally, a near-wall universality (4.1) is obtained independent of both Reynolds number and flow geometries. In addition, a wake flow modification in TBL is introduced for $\langle ww\rangle^+$ and p'^+, which shows close agreement with data towards the boundary layer edge.

There is no gainsaying that more and better data are required to put all these results on a firmer foundation. It is exciting to await cleaner data at higher Reynolds numbers with improved resolution.

Acknowledgement. We thank all the authors cited in the figures for making their data available. We appreciate the suggestion of P. Monkewitz on the analysis leading to (3.9).

Funding. X.C. acknowledges the support by the National Natural Science Foundation of China (grant numbers 12072012, 92252201 and 11721202); and the Fundamental Research Funds for the Central Universities.

Declaration of interests. The authors report no conflict of interest.

Author ORCIDs.
Xi Chen https://orcid.org/0000-0002-4702-8735;
Katepalli R. Sreenivasan https://orcid.org/0000-0002-3943-6827.

References

Bradshaw, P. 1967 'Inactive' motion and pressure fluctuations in turbulent boundary layers. *J. Fluid Mech.* **30**, 241–258.

Chen, X., Hussain, F. & She, Z.S. 2019 Non-universal scaling transition of momentum cascade in wall turbulence. *J. Fluid Mech.* **871**, R2.

Chen, X. & Sreenivasan, K.R. 2021 Reynolds number scaling of the peak turbulence intensity in wall flows. *J. Fluid Mech.* **908**, R3.

Chen, X. & Sreenivasan, K.R. 2022*a* Law of bounded dissipation and its consequenes in turbulent wall flows. *J. Fluid Mech.* **933**, A20.

Chen, X. & Sreenivasan, K.R. 2022*b* Finite-Reynolds-number asymptotics of wall-turbulence fluctuations. In *75th Annual Meeting of the Division of Fluid Dynamics, Indianapolis, Indiana*, vol. 67, abstract no. J26.00009.

Chin, C., Philip, J., Klewicki, J., Ooi, A. & Marusic, I. 2014 Reynolds-number-dependent turbulent inertia and onset of log region in pipe flows. *J. Fluid Mech.* **757**, 747–769.

DeGraaff, D.B. & Eaton, J.K. 2000 Reynolds-number scaling of the flat plate turbulent boundary layer. *J. Fluid Mech.* **422**, 319–346.

Diaz-Daniel, C., Laizet, S. & Vassilicos, J.C. 2017 Wall shear stress fluctuations: mixed scaling and their effects on velocity fluctuations in a turbulent boundary layer. *Phys. Fluids* **29**, 055102.

Gerolymos, G.A. & Vallet, I. 2023 Scaling of pressure fluctuations in compressible turbulent plane channel flow. *J. Fluid Mech.* **958**, A19.

Hoyas, S. & Jimenez, J. 2006 Scaling of the velocity fluctuations in turbulent channels up to $Re_\tau = 2003$. *Phy. Fluids* **18**, 011702.

Hoyas, S., Oberlack, M., Alcantara-Avila, F., Kraheberger, S.V. & Laux, J. 2022 Wall turbulence at high friction Reynolds numbers. *Phys. Rev. Fluids* **7**, 014602.

Hu, R., Dong, S. & Vinuesa, R. 2023 General attached eddies: scaling laws and cascade self-similarity. *Phys. Rev. Fluids* **8**, 044603.

Hultmark, M. 2012 A theory for the streamwise turbulent fluctuations in high Reynolds number pipe flow. *J. Fluid Mech.* **707**, 575–584.

Hultmark, M., Vallikivi, M., Bailey, S.C.C. & Smits, A.J. 2012 Turbulent pipe flow at extreme Reynolds numbers. *Phys. Rev. Lett.* **108**, 094501.

Hwang, Y. & Eckhardt, B. 2020 Attached eddy model revisited using a minimal quasi-linear approximation. *J. Fluid Mech.* **894**, A23.

Hwang, Y., Hutchins, N. & Marusic, I. 2022 The logarithmic variance of streamwise velocity and k^{-1} conundrum in wall turbulence. *J. Fluid Mech.* **933**, A8.

Iwamoto, K., Suzuki, Y. & Kasagi, N. 2002 Database of fully developed channel flow. *Tech. Rep.* ILR-0201, see http://www.thtlab.t.utokyo.ac.jp. Japan.

Jimenez, J., Hoyas, S., Simens, M.P. & Mizuno, Y. 2010 Turbulent boundary layers and channels at moderate Reynolds numbers. *J. Fluid Mech.* **657**, 335–360.

Klewicki, J.C. 2022 Bounded dissipation predicts finite asymptotic state of near-wall turbulence. *J. Fluid Mech.* **940**, F1.

Klewicki, J.C., Priyadarshana, P.J.A. & Metzger, M.M. 2008 Statistical structure of the fluctuating wall pressure and its in-plane gradients at high Reynolds number. *J. Fluid Mech.* **609**, 195–220.

Laval, J.-P., Vassilicos, J.C., Foucaut, J.-M. & Stanislas, M. 2017 Comparison of turbulence profiles in high-Reynolds-number turbulent boundary layers and validation of a predictive model. *J. Fluid Mech.* **814**, R2.

LEE, M. & MOSER, R.D. 2015 Direct numerical simulation of turbulent channel flow up to $Re_\tau = 5200$. *J. Fluid Mech.* **774**, 395–415.

MARUSIC, I., BAARS, W.J. & HUTCHINS, N. 2017 Scaling of the streamwise turbulence intensity in the context of inner–outer interactions in wall turbulence. *Phys. Rev. Fluids* **2**, 100502.

MARUSIC, I., MCKEON, B.J., MONKEWITZ, P.A., NAGIB, H.M., SMITS, A.J. & SREENIVASAN, K.R. 2010 Wall-bounded turbulent flows at high Reynolds numbers: recent advances and key issues. *Phys. Fluids* **22**, 065103.

MARUSIC, I. & MONTY, J.P. 2019 Attached eddy model of wall turbulence. *Annu. Rev. Fluid Mech.* **51**, 49–74.

MARUSIC, I., MONTY, J.P., HULTMARK, M. & SMITS, A.J. 2013 On the logarithmic region in wall turbulence. *J. Fluid Mech.* **716**, R3.

MENEVEAU, C. & MARUSIC, I. 2013 Generalized logarithmic law for high-order moments in turbulent boundary layers. *J. Fluid Mech.* **719**, R1.

METZGER, M.M. & KLEWICKI, J. 2001 A comparative study of near-wall turbulence in high and low Reynolds number boundary layers. *Phys. Fluids* **13**, 692–701.

METZGER, M., MCKEON, B.J. & HOLMES, H. 2007 The near-neutral atmospheric surface layer: turbulence and non-stationarity. *Phil. Trans. R. Soc. Lond.* A **365** (1852), 859–876.

MILLIKAN, C.M. 1938 A critical discussion of turbulent flows in channels and circular tubes. In *Proc. 5th Intl Congress of Applied Mechanics*, pp. 386–392. John Wiley and Sons.

MONKEWITZ, P.A. 2022 Asymptotics of streamwise Reynolds stress in wall turbulence. *J. Fluid Mech.* **931**, A18.

MONKEWITZ, P.A. 2023 Reynolds number scaling and inner-outer overlap of stream-wise Reynolds stress in wall turbulence. *J. Fluid Mech.* (submitted) arXiv:2307.00612.

MONKEWITZ, P.A. & NAGIB, H.M. 2015 Large-Reynolds-number asymptotics of the streamwise normal stress in zero-pressure-gradient turbulent boundary layers. *J. Fluid Mech.* **783**, 474–503.

MONKEWITZ, P.A. & NAGIB, H.M. 2023 The hunt for the Kármán "constant" revisited. *J. Fluid Mech.* **967**, A15.

MOSER, R.D., KIM, J. & MANSOUR, N.N. 1999 Direct numerical simulation of turbulent channel flow up to $Re_\tau = 590$. *Phys. Fluids* **11**, 943–945.

NAGIB, H.M., CHAUHAN, K.A. & MONKEWITZ, P.A. 2007 Approach to an asymptotic state for zero pressure gradient turbulent boundary layers. *Phil. Trans. R. Soc.* A **365**, 755–770.

NAGIB, H.M., MONKEWITZ, P.A., MASCOTELLI, L., FIORINI, T., BELLANI, G., ZHENG, X. & TALAMELLI, A. 2017 Centerline Kármán "constant" revisited and contrasted to log-layer Kármán constant at CICLoPE. In *10th International Symposium on Turbulence and Shear Flow Phenomena (TSFP10), Chicago, USA*.

NAGIB, H.M., MONKEWITZ, P.A. & SREENIVASAN, K.R. 2022 Reynolds number required to accurately discriminate between proposed trends of peak normal stress in wall turbulence. In *75th Annual Meeting of the Division of Fluid Dynamics, Indianapolis, Indiana,* vol. 67, abstract no. Q13.00006.

NILS, T.B. 2021 Scaling of global properties of fluctuating streamwise velocities in pipe flow: impact of the viscous term. *Phys. Fluids* **33**, 125109.

ONO, M., FURUICHI, N., WADA, Y., KURIHARA, N. & TSUJI, Y. 2022 Reynolds number dependence of inner peak turbulence intensity in pipe flow. *Phys. Fluids* **34**, 045103.

PANTON, R.L., LEE, M. & MOSER, R.D. 2017 Correlation of pressure fluctuations in turbulent wall layers. *Phys. Rev. Fluids* **2**, 094604.

PERRY, A.E., HENBEST, S. & CHONG, M.S. 1986 A theoretical and experimental study of wall turbulence. *J. Fluid Mech.* **165**, 163–199.

PIROZZOLI, S., ROMERO, J., FATICA, M., VERZICCO, R. & ORLANDI, P. 2021 One-point statistics for turbulent pipe flow up to $Re_\tau \approx 6000$. *J. Fluid Mech.* **926**, A28.

PULLIN, D.I., INOUE, M. & SAITO, N. 2013 On the asymptotic state of high Reynolds number, smooth-wall turbulent flows. *Phys. Fluids* **25**, 015116.

SAMIE, M., MARUSIC, I., HUTCHINS, N., FU, M.K., FAN, Y., HULTMARK, M. & SMITS, A.J. 2018 Fully resolved measurements of turbulent boundary layer flows up to $Re_\tau = 20\,000$. *J. Fluid Mech.* **851**, 391–415.

SCHLATTER, P. & ÖRLÜ, R. 2010 Assessment of direct numerical simulation data of turbulent boundary layers. *J. Fluid Mech.* **659**, 116–126.

SCHLATTER, P., ÖRLÜ, R., LI, Q., BRETHOUWER, G., FRANSSON, J.H.M., JOHANSSON, A.V., ALFREDSSON, P.H. & HENNINGSON, D.S. 2009 Turbulent boundary layers up to $Re_\theta = 2500$ studied through simulation and experiment. *Phys. Fluids* **11**, 051702.

SCHLATTER, P., LI, Q., BRETHOUWER, G., JOHANSSON, A.V. & HENNINGSON, D.S. 2010 Simulations of spatially evolving turbulent boundary layers up to $Re_\theta = 4300$. *Intl J. Heat Fluid Flow* **31** (3), 251–261.

SHE, Z.S., CHEN, X. & HUSSAIN, F. 2017 Quantifying wall turbulence via a symmetry approach: a Lie group theory. *J. Fluid Mech.* **827**, 322–356.

SILLERO, J.A., JIMENEZ, J. & MOSER, R. 2013 One-point statistics for turbulent wall-bounded flows at Reynolds numbers up to $\delta^+ = 2000$. *Phys. Fluids* **25**, 105102.

DE SILVA, C.M., MARUSIC, I., WOODCOCK, J.D. & MENEVEAU, C. 2015 Scaling of second- and higher-order structure functions in turbulent boundary layers. *J. Fluid Mech.* **769**, 654–686.

SKOULOUDIS, N. & HWANG, Y. 2021 Scaling of turbulence intensities up to $Re_\tau = 10^6$ with a resolvent-based quasilinear approximation. *Phys. Rev. Fluids* **6**, 034602.

SMITS, A.J., HULTMARK, M., LEE, M., PIROZZOLI, S. & WU, X.H. 2021 Reynolds stress scaling in the near-wall region of wall-bounded turbulence. *J. Fluid Mech.* **926**, A31.

SMITS, A.J., MCKEON, B.J. & MARUSIC, I. 2011 High-Reynolds number wall turbulence. *Annu. Rev. Fluid Mech.* **43**, 353–375.

SPALART, P.R. & ABE, H. 2021 Empirical scaling laws for wall-bounded turbulence deduced from direct numerical simulations. *Phys. Rev. Fluids* **6**, 044604.

SREENIVASAN, K.R. 1989 The turbulent boundary layer. In *Frontiers in Experimental Fluid Mechanics* (ed. M. Gad-el-Hak), pp. 159–209. Springer.

TSUJI, Y., FRANSSON, J.H.M., ALFREDSSON, P.H. & JOHANSSON, A.V. 2007 Pressure statistics and their scaling in high-Reynolds-number turbulent boundary layers. *J. Fluid Mech.* **585**, 1–40.

VALLIKIVI, M., GANAPATHISUBRAMANI, B. & SMITS, A.J. 2015 Spectral scaling in boundary layers and pipes at very high Reynolds numbers. *J. Fluid Mech.* **771**, 303–326.

VASSILICOS, J.C., LAVAL, J.-P., FOUCAUT, J.-M. & STANISLAS, M. 2015 The streamwise turbulence intensity in the intermediate layer of turbulent pipe flow. *J. Fluid Mech.* **774**, 324–341.

VINCENTI, P., KLEWICKI, J., MORRILL-WINTER, C., WHITE, C.M. & WOSNIK, M. 2013 Streamwise velocity statistics in turbulent boundary layers that spatially develop to high Reynolds number. *Exp. Fluids* **54**, 1629.

WILLERT, C., SORIA, J., STANISLAS, M., KLINNER, J., AMILI, O., EISFELDER, M., CUVIER, C., BELLANI, G., FIORINI, T. & TALAMELLI, A. 2017 Near-wall statistics of a turbulent pipe flow at shear Reynolds numbers up to 40 000. *J. Fluid Mech.* **826**, R5.

WU, X.H. & MOIN, P. 2009 Direct numerical simulation of turbulence in a nominally zero-presure-gradient flat-plate boundary layer. *J. Fluid Mech.* **630**, 5–41.

YANG, X.I.A. & LOZANO-DURÁN, A. 2017 A multifractal model for the momentum transfer process in wall-bounded flows. *J. Fluid Mech.* **824**, R2.

YAO, J., CHEN, X. & HUSSAIN, F. 2022 Direct numerical simulation of turbulent open channel flows at moderately high Reynolds numbers. *J. Fluid Mech.* **953**, A19.

YAO, J., REZAEIRAVESH, S., SCHLATTER, P. & HUSSAIN, F. 2023 Direct numerical simulations of turbulent pipe flow up to $Re_\tau \approx 5200$. *J. Fluid Mech.* **956**, A18.

ZHENG, X.J. & WANG, G.H. 2016 Very large scale motions in the atmospheric surface layer: a field investigation. *J. Fluid Mech.* **802**, 464–489.